Journal of Magnetism and Magnetic Materials 177–181 (1998) 1–11

ELSEVIER

Journal of magnetism and magnetic materials

Plenary paper

Random fields and phase transitions in model magnetic systems

R.J. Birgeneau*

Department of Physics, Massachusetts Institute of Technology, 6-123, Cambridge, MA 02139, USA

Abstract

Random fields occur in a wide variety of physical systems varying from type II superconductors to two-component fluids in a random medium. However, only in model magnetic systems have systematic studies as a function of both temperature and random-field strength been possible. In this article we review recent neutron and magnetic X-ray scattering studies of the magnetic ordering processes in the antiferromagnets $Mn_{0.75}Zn_{0.25}F_2$, $Fe_{0.5}Zn_{0.5}F_2$ and $Fe_{0.75}Co_{0.25}TiO_3$ in an applied magnetic field. These systems should all represent realizations of the three-dimensional random-field Ising model which is the simplest version of the random-field problem in models with discrete symmetry. In all cases on field cooling (FC) the systems evolve continuously from a high-temperature paramagnetic state to a low-temperature antiferromagnetic domain state. However, on cooling to low temperatures in zero field and then applying a field (ZFC) long-range order (LRO) is obtained. On subsequent heating in the three systems the LRO vanishes continuously with a rounded power-law behavior which has been labelled *trompe l'oeil* critical behavior. The width of the transition region scales as H^2. Reconsideration of indirect ZFC specific-heat measurements shows that the observed peaks, previously attributed to equilibrium critical fluctuations, instead arise entirely from a LRO contribution, scaling like dM_s^2/dT, to the measured quantity. Here M_s is the staggered magnetization. These results thus reconcile scattering and bulk property measurements of random-field Ising systems.

Keywords: Random fields; Antiferromagnetism; Phase transitions; Metastability

1. Introduction

One of the major unsolved problems in the study of phase transitions is the behavior of systems with both quenched disorder and competing interactions or fields. The random-field model, proposed originally by Larkin in 1970 [1] to model the defect pinning of vortices in type II superconductors, has proven to be a useful paradigm for this class of problems. The Ising version of this model, the random-field Ising model (RFIM), most simply encapsulates the essential physics of the problem in systems with discrete symmetry. The RFIM has been the focus of intense study over the past two decades. The Hamiltonian for such systems is

$$H = \sum_{\langle ij \rangle} J_{ij} S_i^z S_j^z - \sum_i h_i S_i^z. \quad (1)$$

Here h_i are the random fields, which typically are assumed to average to zero but with a finite variance. Systems with critical behavior which can be modelled by this Hamiltonian include absorbed monolayers on a square substrate, many structural order–disorder transitions, and certain Jahn–Teller systems, all with impurities which pin the order parameter, as well as two component fluids in a random medium.

Initially, much of the theoretical research on the RFIM dealt with the problem of the lower critical dimension, d_l, the dimension at which, in equilibrium, the random-field fluctuations drive the transition temperature to zero. The pioneering theoretical work of Imry and Ma [2] first discussed the competition between the gain in the statistical random-field energy which occurs when a region follows its weak random field and the loss in the Ising interaction energy at the walls of the domain, for the case of compact domain formation in the d-dimensional RFIM. Using simple phenomenological arguments it was concluded that $d_l = 2$ [2]. This competition between the

* Corresponding author. Tel.: +1 617 253 8900; fax: +1 617 253 8901; e-mail: robertjb@mit.edu.

0304-8853/98/$19.00
PII S0304-8853(97)00998-0

domain-wall energy and the random-field energy lies at the heart of the RFIM and has formed the basis of much of the subsequent theoretical work. The value of the lower critical dimension became controversial after arguments based on perturbation theory suggested that $d_l = 3$. After almost a decade of considerable debate a consensus emerged that $d_l = 2$. This view has been supported, in particular, by the rigorous proof of Imbrie [3, 4] that the three-dimensional (3D) RFIM is ordered at $T = 0$.

Initially, systematic experimental studies of RFIM systems seemed to be prohibitively difficult. However, an important breakthrough occurred when Fishman and Aharony [5] pointed out that the application of an external magnetic field along the easy axis of a random antiferromagnet generates a term in the Hamiltonian which behaves like a random field that couples linearly to the order parameter. Random antiferromagnets are ideally suited to the study of the RFIM because the strength of the random field may be continuously varied simply by adjusting the applied field. A variety of experimental techniques have been applied to these systems including neutron and magnetic X- ray scattering, optical birefringence and Faraday rotation, dilatometry, AC susceptibility, SQUID magnetometry, and NMR techniques. Until recently, the scattering and thermodynamic measurements seemed to yield results which were not easily reconciled with each other. However, recent measurements, including especially synchrotron magnetic X-ray scattering studies, have elucidated further the behavior of RFIM systems and, specifically, seem to have resolved this conundrum.

As we shall discuss in this review, experiments reveal that nonequilibrium effects play an essential role in the behavior of RFIM systems. On the one hand, these make both experiment and theory for the RFIM much more difficult; on the other hand, they make the physics much richer and complex. We now have a very detailed empirical description of the equilibrium and hysteretic behavior in a number of model RFIM systems. However, there is, in our view, no satisfactory theory for the behavior in the nonequilibrium regime and especially for the transition from metastability to equilibrium behavior.

In this paper we shall review recent studies of three different model RFIM systems $Mn_{0.75}Zn_{0.25}F_2$ [6–10], $Fe_{0.5}Zn_{0.5}F_2$ [11–15] and $Fe_{0.75}Co_{0.25}TiO_3$ [16, 17] in an applied magnetic field. Neutron scattering experiments are reviewed in Section 2. The time dependence is discussed in Section 3. Magnetic X-ray scattering measurements are reviewed in Section 4. Direct and indirect specific-heat measurements are discussed in Section 5. The critical behavior in the equilibrium paramagnetic state is reviewed in Section 6. Conclusions and our overall perspective are given in Section 7.

2. Neutron scattering

Neutron scattering has played a central role in the elucidation of the phenomenological behavior of RFIM systems. This is because neutrons couple directly to the spin; they are able to probe the antiferromagnetic spin correlations on length scales from ~ 1 to ~ 1000 Å and for energies varying from microvolts to millivolts. Beginning with the pioneering studies in 1980 by Cowley and coworkers of RFIM effects in $Co_{1-x}Zn_xF_2$ [18, 19], a series of neutron scattering experiments have been performed on random antiferromagnets in a field. The most detailed experiments have been carried out on the diluted antiferromagnets $Mn_{1-x}Zn_xF_2$ and $Fe_{1-x}Zn_xF_2$ which are, respectively, weakly and strongly anisotropic two-sublattice Ising antiferromagnets.

Generally, the Ising component of the neutron scattering cross section in a 3D RFIM system may be written as

$$S(\boldsymbol{Q}) = \frac{A\kappa}{(\kappa^2 + q^2)^2} + \frac{B}{\kappa^2 + q^2} + C\delta(\boldsymbol{q}), \tag{2}$$

where $\boldsymbol{q} = \boldsymbol{Q} - \boldsymbol{Q}_{AF}$. The δ function represents any long-range magnetic-order component. The second term corresponds to the longitudinal dynamic susceptibility. The Lorentzian-squared term arises from static fluctuations due to the quenched random-field. Written in this form, A is the integrated intensity for these fluctuations. From the fluctuation dissipation theorem, the structure factor $S(\boldsymbol{Q})$ of Eq. (2) may be written as the sum of two terms, $S(\boldsymbol{Q}) = T\chi_{dis}(\boldsymbol{Q}) + T\chi(\boldsymbol{Q})$, where $\chi_{dis} = \sum_j \langle\sigma_0\rangle\langle\sigma_j\rangle$ and $\chi = \sum_j [\langle\sigma_0\sigma_j\rangle - \langle\sigma_0\rangle\langle\sigma_j\rangle]$, are the so-called disconnected and connected susceptibilities, respectively. In a nonrandom system, for $T > T_c$, $\sum_j \langle\sigma_0\rangle\langle\sigma_j\rangle = 0$ and $S(0) \sim T\chi \sim t^{-\gamma}$. However, in random systems χ_{dis} is no longer zero and a new exponent is defined, $\chi_{dis} \sim t^{-\bar{\gamma}}$. In Section 6, we will discuss experimental measurements of the equilibrium critical fluctuations in the high-temperature paramagnetic region which yield values for γ and $\bar{\gamma}$, together with the correlation length exponent ν, where $1/\kappa \sim t^{-\nu}$. In Eq. (2), we identify the thermal fluctuations, given by parameter B with $\chi(\boldsymbol{Q})$ and the random-field fluctuations, A, with $\chi_{dis}(\boldsymbol{Q})$. In this section we will focus on the evolution of the RFIM from the high-temperature equilibrium paramagnetic state to the low-temperature metastable regime.

A detailed set of neutron experiments in $Mn_{0.75}Zn_{0.25}F_2$ at various fields are reported in Ref. [6–8]. We show in Fig. 1 data obtained at 5.0 T using a triple-axis configuration with energy resolution 20 μeV half-width at half-maximum (HWHM). It was anticipated that the high-energy resolution would eliminate the Lorentzian term in Eq. (2) which is dynamic in character and isolate the Lorentzian squared term which originates from the static-ordered moments induced by the random field.

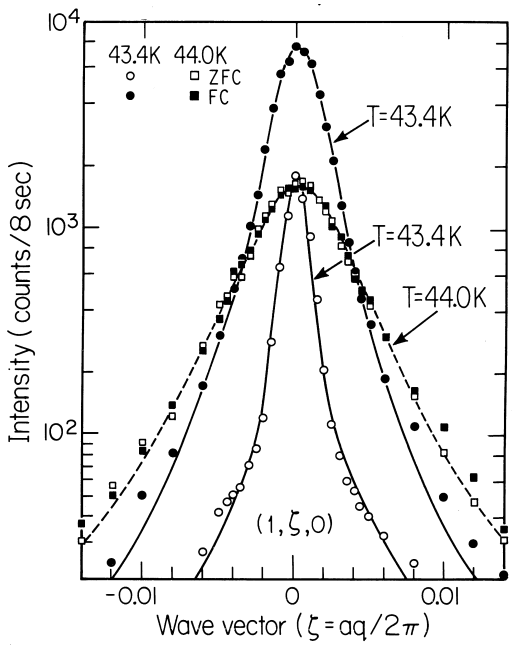

Fig. 1. The neutron scattering observed as a function of wave vector $\boldsymbol{Q} = (1, \zeta, 0)$ in $Mn_{0.75}Zn_{0.25}F_2$ in a field of 5.0 T, with a two-axis configuration. At 44.0 K the results are independent of the previous history but at 43.4 K they are dependent on the history [6–8].

Thermal expansion measurements which were carried out on the same system show a hysteretic peak at $T_c(5.0\ \mathrm{T}) \cong 43.7$ K [20, 21]. The samples used in the neutron and thermal expansion experiments were cut from adjacent sections of the same boule and their $H = 0$ Néel temperatures coincided to within the errors ($T_N(0) = 46.0$ K). As shown in Fig. 1 at 44.0 K $S(\boldsymbol{q})$ is the same for the FC and ZFC procedures. The correlation length $\xi = \kappa^{-1}$ is ~ 200 Å. However, at 43.4 K the spin configuration explicitly depends on the history of the sample. The FC correlation length at 43.4 K is ~ 550 Å whereas the ZFC system has long-range order (LRO).

The results for the inverse correlation length κ from fits to the $H = 5.0$ T neutron data are shown in Fig. 2. For the ZFC data the profiles were fit to the sum of a resolution-limited Gaussian and a Lorentzian squared. The double-arrow in Fig. 2 denotes the transition region. This will be discussed in more detail in Section 4.

These data illustrate the essential behavior of RFIM systems. Above a certain temperature, which we label $T_{eq}(H)$, equilibrium is obtained. Below $T_{eq}(H)$ the physical state of the system depends on the history of the sample. For FC measurements the domains grow progressively in size but saturate at a finite value. However, for ZFC measurements LRO obtains up to $T_{eq}(H)$. The loss of LRO on heating in the ZFC procedure occurs with accompanying Lorentzian-squared fluctuations where the maximum length of these fluctuations which is

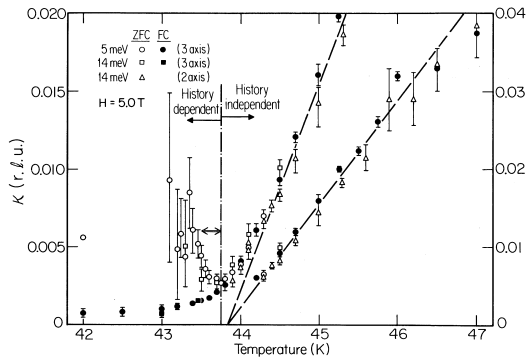

Fig. 2. The temperature dependence of the inverse correlation length, κ, close to the metastability boundary in $Mn_{0.75}Zn_{0.25}F_2$ for data taken with $H = 5.0$ T with FC and ZFC procedures [6–8].

achieved near but below $T_{eq}(H)$ equals the corresponding FC value to within the errors. We shall discuss the detailed behavior in the transition region in Section 4. The critical behavior in the equilibrium region above $T_{eq}(H)$ will be discussed in Section 6.

Results essentially identical to these are obtained in both $Fe_{1-x}Zn_xF_2$ [11–15] and $Fe_{0.75}Co_{0.25}TiO_3$ [16, 17] in an applied magnetic field. The former is a highly anisotropic diluted Ising magnet whereas the latter is a mixture of Ising ($FeTiO_3$) and XY ($CoTiO_3$) magnets. Thus, the behavior shown in Figs. 1 and 2 is generic depending only on the overall 3D Ising symmetry and not on the microscopic details. We will discuss current models for this hysteretic behavior, especially in the transition region, in Section 5.

3. Time dependence

The statement that $d_l = 2$ requires that the FC domain state we observe in these 3D RFIM magnets is a nonequilibrium state and that in equilibrium one expects true LRO. This, in turn, suggests that the FC domains should expand as a function of time. Theories which assume an instantaneous quench from the paramagnetic phase into the 'ordered' region predict that the domains will grow logarithmically with time and further that they cannot then contract unless one crosses the phase boundary [22–24]. The latter is in agreement with experiment. The quenched domain size is predicted to scale like

$$\xi \sim \frac{JT}{H^2} \ln(t/\tau), \tag{3}$$

where τ is a microscopic time which cannot be shorter that $K/J \sim 10^{-11}$ s. The linear dependence on T in Eq. (3) is not observed in field cooling; rather ξ saturates at relatively high temperatures; presumably this reflects

the difference between field-cooling and the instantaneous quench procedure assumed in deriving Eq. (3). In $Fe_xZn_{1-x}F_2$ at low temperatures ξ does indeed scale like H^{-2} [25]. However, in $Co_{0.35}Zn_{0.65}F_2$ the exponent is 3.6 ± 0.4 [18, 19] while in $Mn_{0.5}Zn_{0.5}F_2$ it is 3.4 ± 0.4 [6–8] although recent experiments at small fields on this latter system give a value closer to 2 [14]. The order of magnitude of ξ is given correctly by Eq. (3).

The most important qualitative feature of Eq. (3) is that ξ should increase logarithmically with time. By rapidly quenching a sample through the phase boundary it is possible to measure ξ for times varying between $\sim 10^2$ and $\sim 10^5$ s – enough to test Eq. (3) with $\tau = 10^{-11}$ s. Birgeneau et al. [6–8] report an experiment carried out for $H = 7.0$ T in $Mn_{0.75}Zn_{0.25}F_2$ where the sample was quenched from 0.4 K above the phase boundary to 0.4 K below the boundary. As may be seen from Fig. 3, the ratio of domain sizes at 5.4×10^4 and 6.0×10^2 s was measured to be 1.01 ± 0.03 compared with a minimum ratio of 1.14 predicted by the logarithmic law, Eq. (3). Thus, logarithmic expansion with time of the FC domain radius is excluded. A series of additional field cooling or field lowering experiments in $Mn_{0.75}Zn_{0.25}F_2$ and $Mn_{0.5}Zn_{0.5}F_2$ confirm this conclusion [6–8].

This apparent contradiction with theory was addressed by Natterman and Vilfan [26]. They concluded that the absence of measurable $\ln(t/\tau)$ domain expansion behavior in $Mn_{1-x}Zn_xF_2$ was due to the weak anisotropy and consequent broad domain walls in that system. They predicted that the logarithmic growth in time of the domains should be observable in a narrow domain-wall system such as $Fe_{1-x}Zn_xF_2$. They further predicted that the time dependence should be generalized to $\ln(t/\tau)^{-\psi}$.

Recently, Feng and co-workers [13] have studied the time dependence of the FC domain size in the highly anisotropic diluted 3D Ising magnet $Fe_{0.5}Zn_{0.5}F_2$. They have, in addition, measured the time dependence of the excess magnetization $M_{ex} = M_{FC} - M_{ZFC}$ where M_{FC} and M_{ZFC} are the magnetizations at a given field and temperature after field cooling and zero-field cooling, respectively. Heuristically, M_{ex} should provide a measure of the excess magnetization in the FC domain walls; a phenomenological argument suggests that M_{ex} should scale like ξ^{-1} possibly raised to a power ψ depending on the fractal nature of the domain walls [26, 27].

Fig. 4 shows a comparison of the inverse correlation length κ obtained directly using neutron scattering techniques and M_{ex} determined by SQUID measurements

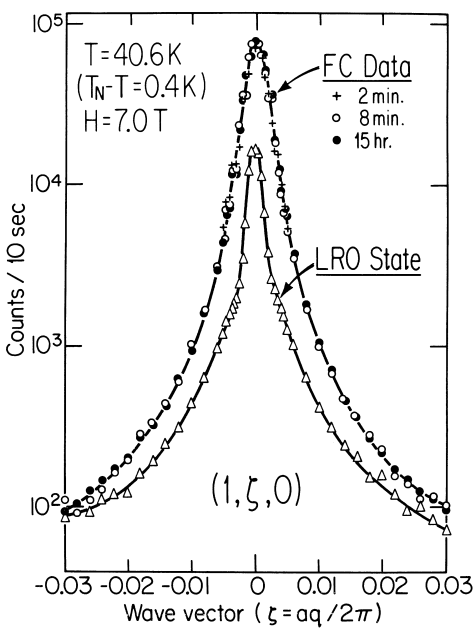

Fig. 3. Scattering profiles in $Mn_{0.75}Zn_{0.25}F_2$ in a field $H = 7.0$ T. The LRO-state data were obtained by the ZFC procedure. The FC data were obtained by first raising the temperature of the ZFC state to 41.4 K, and then cooling it rapidly to 40.6 K. The solid lines are guides to the eye [6–8].

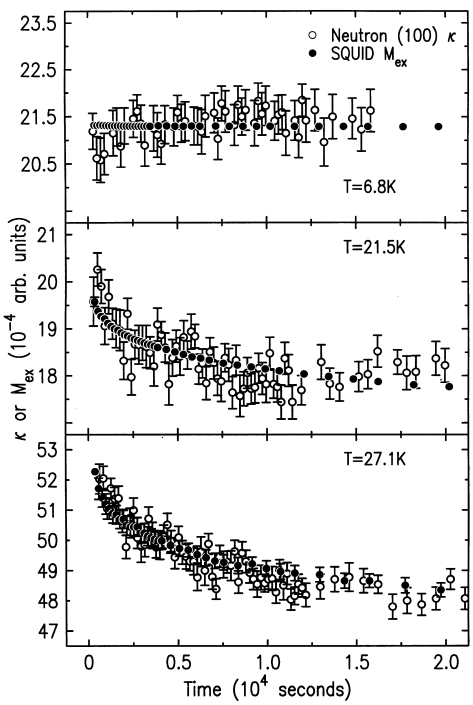

Fig. 4. Comparison of the time dependence of the inverse correlation length, κ, as measured by neutron scattering and the excess magnetization from domain walls M_{ex} as measured by the SQUID for three temperatures below the transition in $Fe_{0.5}Zn_{0.5}F_2$ in a field of 5.5 T. The M_{ex} values have been rescaled according to the neutron scattering κ. Both techniques show frozen dynamics at low temperatures. At higher temperatures, the two techniques also agree, suggesting that the fractal properties of the domains do not change noticeably while the average size of the domain grows with time [13].

in $Fe_{0.5}Zn_{0.5}F_2$, taken at the same temperatures at $H = 5.5$ T. At $T = 6.8$ K, both techniques show that the magnetic domains are frozen. At $T = 21.5$ and 27.1 K, κ and M_{ex} undergo a similar percentage of decay over the same period of time. Detailed fits show that the decay is consistent with the simple logarithmic form $\ln(t/\tau)$, i.e., $\psi = 1$ although the uncertainties in the exponent are large. More generally, from detailed studies of M_{ex} it is found that ψ is typically much less than 1 at low fields, increasing to 1 at higher fields [13].

In brief, then, the experiments of Feng et al. [13] confirm the predictions of Natterman and Vilfan [26]. Specifically, in narrow domain-wall systems logarithmic expansion of the FC metastable domains is indeed directly observed. The measurements also confirm the close association between the FC domain-wall radius and the excess magnetization $M_{ex} = M_{FC} - M_{ZFC}$.

4. Magnetic X-ray scattering

Neutron scattering studies of the ZFC behavior are compromised because the diffraction is severely affected by extinction. Thus it is not possible to measure quantitatively the temperature evolution of the order parameter, at least outside of the transition region. An alternative experimental approach made possible by the advent of dedicated synchrotron sources is to study the magnetic correlations using magnetic X-ray scattering. This technique is complementary to neutron scattering with several important strengths. First, the small cross section results in extinction-free scattering, so that the order parameter may be reliably determined. This is of particular importance in the work discussed here. Second, the small penetration depth of X-rays, typically on the order of 2 μm, may reduce the effect of concentration gradients. Third, the high reciprocal space resolution allows large length scales to be probed. Fourth, the relatively poor energy resolution (~ 10 eV) ensures integration over all relevant thermal fluctuations. Fifth, though not pertinent to this work, the contributions due to the orbital and spin magnetic moments may be distinguished through polarization analysis.

Extensive studies of each of $Mn_{1-x}Zn_xF_2$ [9, 10], $Fe_{1-x}Zn_xF_2$ [11, 12] and $Fe_{1-x}Co_xTiO_3$ [16, 17] in an applied field have been carried out using magnetic X-ray scattering techniques. The FC results so-obtained agree in detail with those measured using neutron scattering techniques. We will not review those results here. Instead, we will focus on the ZFC transition behavior. As discussed previously, bulk thermodynamic measurements of properties such as the thermal expansion [14] and the temperature derivative of the uniform magnetization [11, 12, 27] or optical birefringence [28–30] show anomalies on warming from the low-temperature ZFC state. As we shall discuss in Section 5, these anomalies occur just below $T_{eq}(H)$. They have been interpreted by some groups as signalling an equilibrium phase transition with RFIM critical behavior [28–30]. However, it is difficult to reconcile this claimed critical behavior with the fact that the system is manifestly not in equilibrium and with the absence of a divergent magnetic correlation length (cf. Fig. 2).

We discuss first results in $Mn_{0.75}Zn_{0.25}F_2$ [9, 10]. The salient features of the disordering process are shown in Figs. 5 and 6. Representative scans through the (1 0 0) magnetic Bragg peak are shown in Fig. 5 at a series of temperatures for $H = 6.0$ T. The system was initially cooled into the XY phase and then warmed with the field fixed at $H = 6.0$ T. This is equivalent to the ZFC process since the XY phase has true LRO. The peak is well-fit by the resolution function, which is a Lorentzian, for all temperatures up to $T_{eq}(H)$, the metastability boundary. This corresponds to a domain size in excess of 20 000 Å.

Fig. 6 shows the (1 0 0) peak intensity versus temperature for a series of such runs at different fields in two different samples. A remarkable feature of these data is that the behavior is universal for all fields studied. In particular, at low temperatures there is a linear diminution with increasing temperature of the order parameter, crossing over to a power-law-like decay with exponent, $\beta = 0.2 \pm 0.05$, near $T_{eq}(H)$. Further, a careful

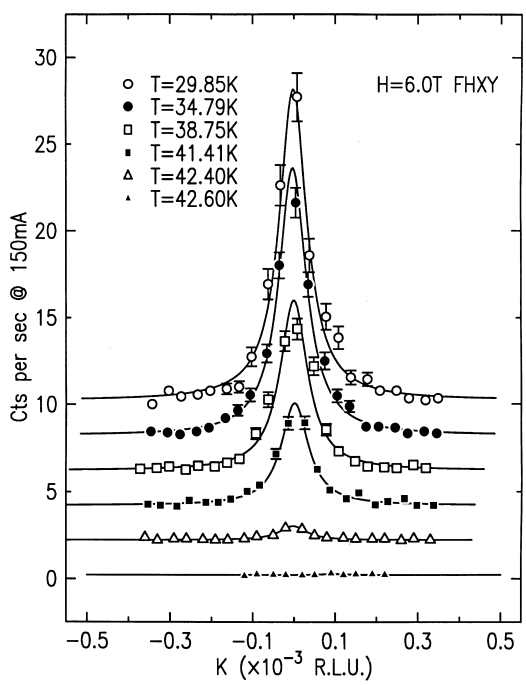

Fig. 5. Representative transverse X-ray scans in $Mn_{0.75}Zn_{0.25}F_2$ taken on warming from the XY phase at $H = 6.0$ T. These data are offset by two counts/s for each successive temperature. The data are well fit by a Lorentzian resolution function of constant width $\kappa = 4 \times 10^{-5}$ r.l.u. [9, 10].

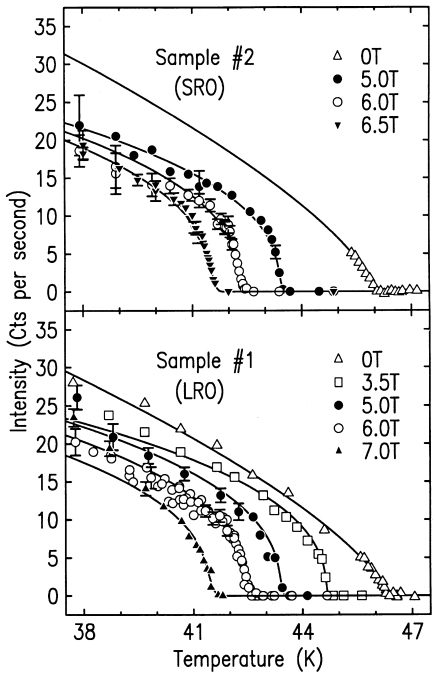

Fig. 6. Order parameter squared versus temperature after ZFC ($H = 3.5$ and 5.0 T) and FHXY ($H = 6.0$, 6.5 and 7.0 T) in two different samples of $Mn_{0.75}Zn_{0.25}F_2$. The solid lines through the $H = 0$ T data are the results of power-law fits $I \sim (T_N - T)^{2\beta}$ with $2\beta = 0.70$. The solid lines through the $H \neq 0$ data are the results of fits to a Gaussian rounded power law, Eq. (4), with $2\beta = 0.40$ and $\sigma_{ZFC}(H) = 0.0034H^2$ (K/T^2) [9, 10].

inspection of the data in the transition region reveals that the transition is not a true power law, but rather it is smeared out. The solid lines in Fig. 6 represent the results of fits to a power law with $\beta = 0.2$ and a Gaussian distribution of transition temperatures;

$$I(T,H) = \frac{1}{\sqrt{\pi\sigma_{ZFC}(H)}}\int\left(\frac{t_c - T}{t_c}\right)^{2\beta} \times \exp\left(-\left(\frac{t_c - T_c(H)}{\sigma_{ZFC}(H)}\right)^2\right) dt_c, \quad (4)$$

from the fits one finds that to within the errors $\sigma_{ZFC}(H) \sim H^2$.

With the knowledge that the width of the transition region scales as H^2, one can construct a scaling plot for these data. That is, by measuring the temperature in units H^2, all of the $H \neq 0$ data should collapse onto a single curve. Fig. 7 displays the data of Fig. 6 as a function of the variable $(T - T_c(H))/H^2$. The relative intensity is then the only free parameter, and is adjusted to optimize the data collapse. The data do indeed collapse onto a single function, shown in the figure as the solid line. The scaling function is a power law with exponent $\beta = 0.2$ with a transition region rounded as H^2. This has been

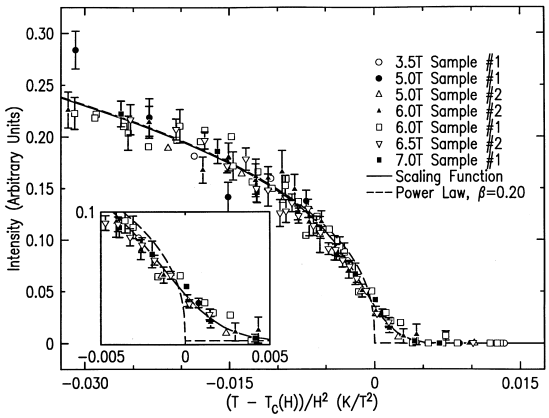

Fig. 7. Scaling of the ZFC data in the transition region in $Mn_{0.75}Zn_{0.25}F_2$. The data are plotted as a function of the scaling variable $(T - T_c(H))/H^2$; the relative intensity is then the only free parameter and is adjusted to optimize the data collapse [9, 10].

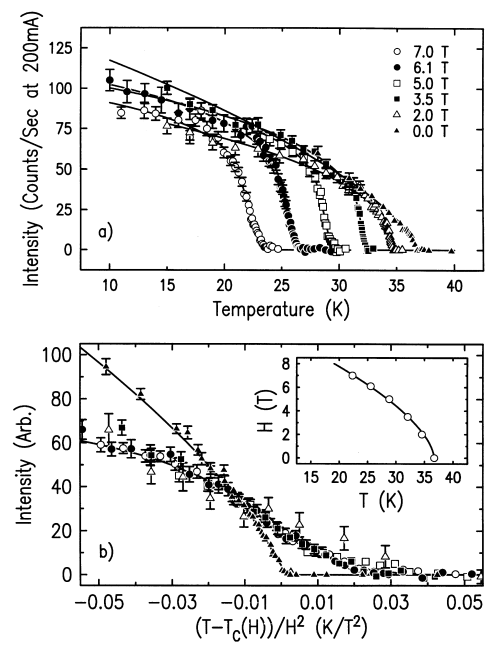

Fig. 8. (a) The ZFC order parameter squared in $Fe_{0.5}Zn_{0.5}F_2$ as measured at the (1 0 0) position with X-rays for five fields and $H = 0$ T. For $H \neq 0$, the data are well described by a power-law-like behavior with a broadened transition region. The broadening is modelled by a Gaussian distribution of transition temperatures of width $\sigma_{ZFC}(H) \propto AH^2$, Eq. (4). (b) The $H \neq 0$ data of (a) replotted as a function of the temperature interval away from $T_c(H)$ as measured in units of H^2. This illustrates the rounding of the transition which is attributed to nonequilibrium effects arising from extreme critical slowing down and the universal scaling behavior of the *trompe l'oeil* critical phenomena. The inset shows the phase boundary of $Fe_{0.5}Zn_{0.5}F_2$ as determined from the X-ray fits [11, 12].

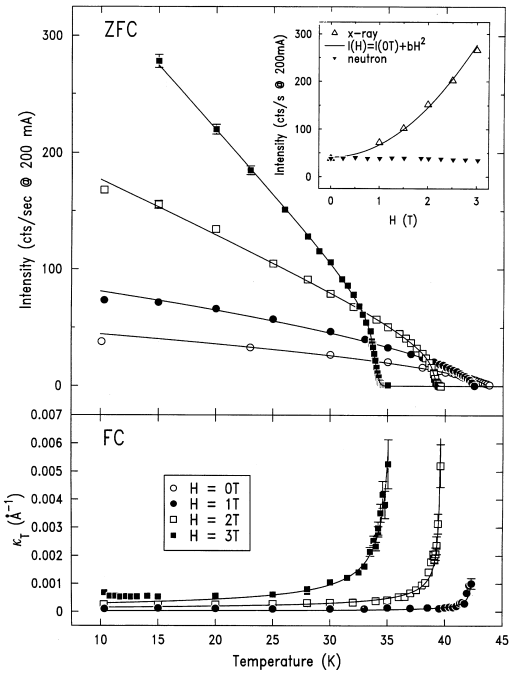

Fig. 9. RFIM behavior of $Fe_{0.75}Co_{0.25}TiO_3$ in a magnetic field. The upper panel shows the (1, 1, 1.5) Bragg intensity after ZFC. The solid lines for $H \neq 0$ are the results of fits to the *trompe l'oeil* model, Eq. (4). The $H = 0$ line is the result of a fit to a simple power law with $\beta_{\|} = 0.36(3)$. The inset shows the (1, 1, 1.5) intensity for $T = 15$ K as a function of field for X-rays and neutrons. The H dependence in the X-ray cross section originates in a subtle coupling term which scales like $MM_s\rho_s$ where M is the magnetization, M_s the staggered magnetization and ρ_s the staggered charge density. The bottom panel shows the FC inverse correlation length κ_T for varied fields [16, 17].

labelled *trompe l'oeil* critical behavior since the behavior simulates ordinary critical phenomena at a second-order phase transition but, in fact, represents escape from metastability [9, 10].

A similar set of experiments and analysis was carried out in $Fe_{0.5}Zn_{0.5}F_2$ [11, 12]. The results are shown in Fig. 8. Again one finds that $\sigma_{ZFC}(H) \sim H^2$. This once more enables one to construct a scaling plot as shown in the bottom panel of Fig. 8. The best fit of Eq. (4) to the scaled data yields $\beta = 0.15 \pm 0.05$. As shown in Fig. 9, similar results are obtained in $Fe_{0.75}Co_{0.25}TiO_3$ although in that case the data are more complicated because of a novel coupling between the magnetization, the staggered magnetization and the staggered charge density which affects the magnetic superlattice X-ray cross section [16, 17].

We should emphasize that Eq. (4) is not unique. Indeed, as pointed out by Wong [31] and Hill et al. [32] a model assuming a mean-field first-order transition rounded like H^2 can also describe the data. Currently there is no real theory for the observed *trompe l'oeil* behavior.

5. Scattering, direct and indirect heat capacity data

One of the most important experimental issues for the RFIM has been how one reconciles X-ray and neutron scattering data with direct and indirect heat capacity results. Recent work seems to have resolved this conundrum [11, 12]. We show in Fig. 10 results of neutron and X-ray scattering measurements on an identical sample of $Fe_{0.5}Zn_{0.5}F_2$ in a field of 6.1 T. The X-ray and neutron thermometer scales were normalized at $H = 0$ T ($T_N = (0) = 36.8$ K), and no further temperature-scale correction was made in comparing the neutron and X-ray data at 6.1 T. Fig. 10 contains several important results. First, it shows that neutron and magnetic X-ray scattering yield identical results for M_s^2 in the transition region. Second, the ZFC fluctuation correlation length is a maximum at $T_c(H)$, and this length equals the corresponding FC value at all temperatures $\geqslant T_c(H)$. This was also seen earlier in measurements in $Mn_{0.75}Zn_{0.25}F_2$ (Fig. 2). Concomitantly, the critical scattering amplitude measured at $(1, -0.003, 0)$ is a maximum at $T_c(H)$.

Fig. 11 shows the results of SQUID and neutron measurements in $Fe_{0.5}Zn_{0.5}F_2$ at 5 T [11, 12]. The SQUID data were taken on a small piece cut from the

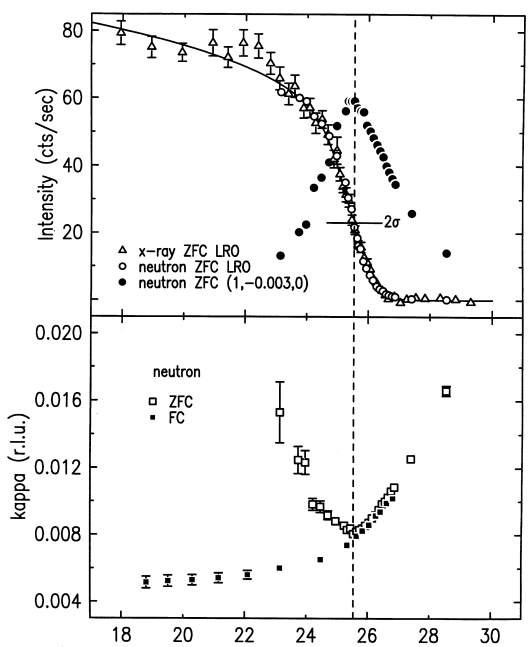

Fig. 10. Top panel: X-ray and neutron magnetic intensities in $Fe_{0.5}Zn_{0.5}F_2$ for $H = 6.1$ T. The solid line is the result of a fit to the rounded power law of Eq. (4) with $T_c(6.1\text{ T}) = 25.54$ K (dashed line) and $\sigma(6.1\text{ T}) = 0.9$ K. Bottom panel: Inverse correlation length versus temperature on FC and ZFC [11, 12].

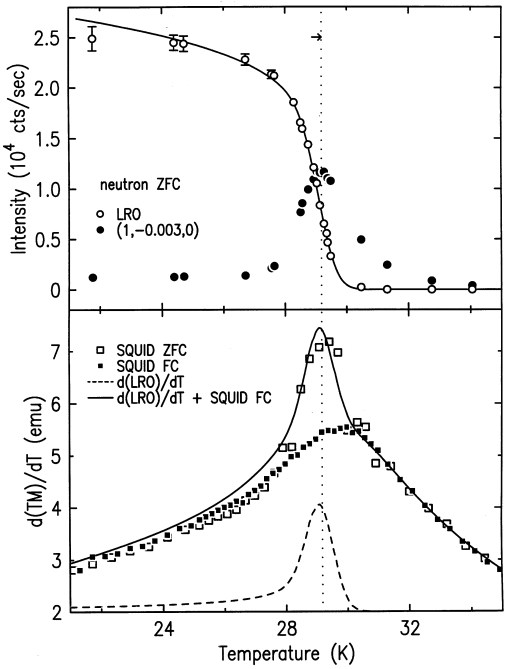

Fig. 11. Top panel: neutron scattering intensity at (1, 0, 0) (LRO) and (1, −0.003, 0) at $H = 5.0$ T. The solid line is the result of a fit to the *trompe l'oeil* rounded power-law form, Eq. (4). The small arrow at the top indicated the 0.3 K shift in the neutron data temperature scale. Bottom panel: FC and ZFC data for $\mathrm{d}(TM)/\mathrm{d}T$ at $H = 5.0$ T [11, 12].

neutron sample. They agree in detail with previous results by Lederman and co-workers [27]. The neutron data are analogous to those shown in Fig. 10 at 6.1 T. The temperature derivative of the SQUID magnetization shows a sharp peak on ZFC, but not FC. The temperature scales of the neutron and magnetization data have again been normalized at $H = 0$ T. The net accuracy of this normalization is ± 0.3 K. In plotting the data at 5 T in Fig. 11, the neutron temperature scale has been shifted by 0.3 K, as indicated by the small arrow at the top of the figure. This is based on the physically compelling argument that $\mathrm{d}(TM)/\mathrm{d}T$ should have its maximum at the same temperature as that at which the correlation length is a maximum. In any case, the temperature-scale shift is within the combined temperature uncertainties, and its omission has no important effect on the overall argument.

In Refs. [11, 12] it was hypothesized that for indirect heat-capacity techniques for RFIM systems there may be a term of the form $\mathrm{d}M_s^2/\mathrm{d}T$. The argument was based on general phenomenological considerations for probes where the response is determined by short-range spin–spin correlations. In fact, such a term has been hypothesized previously by many authors for different kinds of measurements in other kinds of systems and has been observed in a number of cases. It was further hypothesized that the thermal contribution to $\mathrm{d}(TM)/\mathrm{d}T$, which is determined by short-range effects, would not be very different for FC and ZFC measurements. Therefore, as a first approximation, the ZFC $\mathrm{d}(TM)/\mathrm{d}T$, should equal the FC result augmented by the $\mathrm{d}M_s^2/\mathrm{d}T$ contribution. The solid line in the bottom panel of Fig. 11 is the result of such an analysis. In this case, only the amplitude of the $\mathrm{d}M_s^2/\mathrm{d}T$ contribution (dashed line) has been varied, and there has been no further adjustment in the temperature scale. Clearly this simple model describes the ZFC $\mathrm{d}(TM)/\mathrm{d}T$ data very well. Similar agreement is obtained at all other fields; in each case the adjustment of the temperature scales to match the peak temperatures is well within the temperature uncertainties. The evident good agreement is compelling evidence that the basic model is correct.

In order to test these ideas further, direct heat-capacity measurements were carried out by Feng and Ramirez both on samples of $Fe_{0.5}Zn_{0.5}F_2$ taken from the same boule as the samples used in the above work, and on crystals of $Mn_{0.75}Zn_{0.25}F_2$ [11, 12, 15]. The above model necessitates that the direct heat capacity, which is sensitive to the local spin configuration and not to the LRO, should show little hysteresis. In the top panel of Fig. 12, direct heat-capacity data taken on $Fe_{0.5}Zn_{0.5}F_2$ at $H = 1.5$ T, and 5.5 T are displayed. These data were taken using a semiadiabatic technique. The time scale for each datum point is ~ 20 s. There is no observable hysteresis in either data set. This demonstrates that the FC and ZFC thermal fluctuations are closely similar. Identical results are obtained in $Mn_{0.75}Zn_{0.25}F_2$ [15]. It is clear that the ZFC peak of indirect heat-capacity methods is not indicative of the true heat capacity.

Finally, these ideas have been tested on published birefringence data, as shown in the bottom panels in Fig. 12. In Fig. 12b, we show data of Ferreira et al. [28–30] taken on a sample of $Fe_{0.46}Zn_{0.54}F_2$ of very high quality. In this case, the solid line is the X-ray scaling function with the width taken from the H^2 scaling law of Fig. 8. The FC data are used for the background arising from the noncritical fluctuations. $T_c(H)$ was adjusted slightly from the value determined in the X-ray experiments on $Fe_{0.5}Zn_{0.5}F_2$. Again the agreement is good. Finally, in Fig. 12c similar data and analysis for $Fe_{0.6}Zn_{0.4}F_2$ are shown [11, 12, 28–30]. In this case, the coefficient of the H^2 width is fitted at $H = 4$ T. Once more the model describes the ZFC birefringence data well.

The above analysis removes one of the major stumbling blocks in understanding the phenomenology of RFIM systems. In general, it is now clear that there are three important temperatures: $T_{eq}(H) > T_c(H) > T_N(H)$. $T_{eq}(H)$ is the onset temperature for metastability effects. $T_c(H)$ is the midpoint of the transition region of the diminution of the order parameter after ZFC. $T_N(H)$ is the equilibrium Néel temperature. So far no true

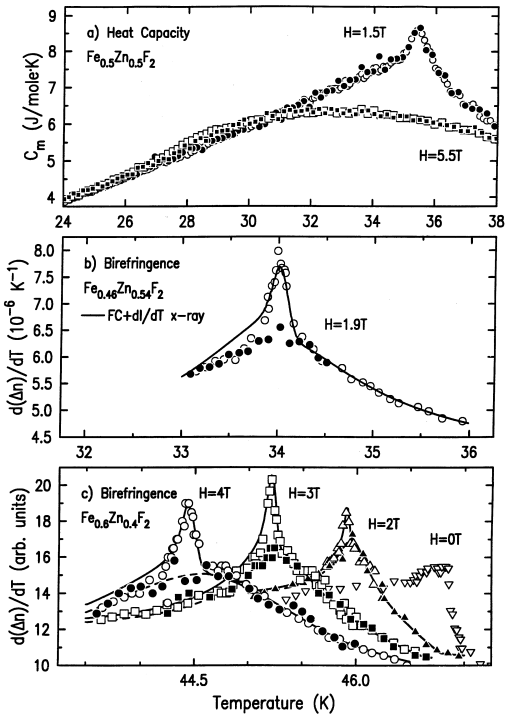

Fig. 12. (a) Heat capacity of $Fe_{0.5}Zn_{0.5}F_2$. There is no evidence of hysteresis on FC and ZFC, nor is there any sign of critical heat capacity in the ZFC data. (b) Optical birefringence data taken from Ferreira et al. [29] for $Fe_{0.46}Zn_{0.54}F_2$. The solid line is the FC data plus the contribution from the dM_s^2/dT term. (c) Similar results and analysis for $Fe_{0.6}Zn_{0.4}F_2$ (Refs. [28–30]). In each panel, the open symbols are ZFC data and the closed symbols are FC results [11, 12].

equilibrium phase transition in the bulk has been observed in RFIM systems. A transition to LRO on FC has been observed in certain samples in the near-surface region ($\sim 2\,\mu$m) using X-ray scattering techniques [9, 10, 14]. However, the interpretation of these experiments is still problematical so we do not discuss them explicitly here.

How does one understand the breakdown of equilibrium at $T_{eq}(H)$? A phenomenological model has been introduced by Villain [33] and Fisher [34]. The Villain–Fisher picture is as follows. For a given correlated volume, there is only one thermally populated minimum. Thermal fluctuations in this minimum are small because of the steep curvature in the free energy. However, on rare occasions, with probability T/ξ^θ two minima occur within a correlated volume which differ in energy only by order T. In such cases, the equilibrium fluctuations may be thermally activated over the free-energy barrier. To achieve such a reversal of a block of spins of size R, a free-energy barrier of height $\omega(R) \approx R^\theta$ must be overcome. R^θ is the random-field energy of a volume R^d (the surface tension vanishes as $T \to T_c$) and θ is the exponent which modifies the hyperscaling relation to $(d-\theta)\nu = 2-\alpha$. Arrhenius' law then implies that the characteristic relaxation time of the system close to the transition, i.e., the time to flip a correlated volume, is

$$\tau \approx \tau_0 \exp(C\xi^\theta), \tag{5}$$

where τ_0 and C depend on the random-field strength. The 'activated dynamics' of Eq. (5) result in extreme critical slowing down and the system cannot equilibrate on experimentally accessible time scales, as $\xi \to \infty$. $T_{eq}(H)$ then is the temperature above $T_N(H)$ at which τ exceeds laboratory measurement time scales.

The ZFC *trompe l'oeil* critical behavior then may be understood as follows: just as extreme critical slowing down prevents the attainment of equilibrium on field cooling, activated dynamics with the concomitant extreme critical slowing down will also operate on warming the ZFC state. Thus, as the temperature is increased to $T \lesssim T_N(H)$, the system will fall out of equilibrium, at least on experimentally relevant time scales, and the correlation length will saturate, as is observed experimentally. The system will not be able to relax fully until it has passed through the critical region to reach the high-temperature equilibrium phase. This leads to a qualitative picture of the process in which the LRO is destroyed through 'flipping' of domains with successively larger sizes. The maximum rate of change occurs at the center of the *trompe l'oeil* Gaussian distribution which is when the size of the volume being flipped becomes approximately equal to the FC domain size at that temperature. As found experimentally, the rounding of the transition may then be understood as a finite-size effect, in which the growth of the correlation length in the transition region is limited by the random fields to the FC domain size [6–12].

6. Equilibrium critical behavior

Because of the onset of metastability at $T_{eq}(H)$, which is well above the equilibrium phase transition temperature $T_N(H)$, studies of the asymptotic equilibrium critical behavior in RFIM systems appear not to be possible. Further, the behavior well above $T_N(H)$ is complicated by an anticipated crossover from random exchange to random-field Ising critical behavior. Thus, at best crude estimates of the 3D RFIM critical exponents can be obtained experimentally. Such estimates are nevertheless valuable since the critical behavior of the 3D RFIM is expected to be radically different from that of the uniform or random exchange 3D Ising model, including especially an unusually rapid divergence of the disconnected susceptibility [35, 36].

Feng et al. [14] have carried out a study of the FC behavior in $Fe_{0.5}Zn_{0.5}F_2$ in fields of 5 and 6 T using

two-axis neutron scattering techniques. From deconvolutions of the neutron scattering spectra they are able to extract the inverse correlation length κ, the connected susceptibility $\chi \sim B/\kappa^2$ and the disconnected susceptibility $\chi_{dis} \sim A/\kappa^3$. The results so-obtained at 5 T are shown in Fig. 13. From fits of power laws, $\kappa \sim (T - T_N(H))^{\nu}$, to the κ data they find $\nu = 1.5 \pm 0.3$. With $T_N(H)$ fixed at the value determined from fits to the κ data, they then find for the connected susceptibility $\gamma = 2.6 \pm 0.5$ and for the disconnected susceptibility $\bar{\gamma} = 5.7 \pm 1$. The large errors reflect the strong dependence of the exponents on the choice of $T_N(H)$. Cowley et al. [6–8] have carried out a similar analysis on their data on $Mn_{0.75}Zn_{0.25}F_2$. They find $\nu = 1.4 \pm 0.3$ and $\bar{\gamma} = 4.5 \pm 1$. Thus the experiments in $Fe_{0.5}Zn_{0.5}F_2$ and $Mn_{0.75}Zn_{0.25}F_2$ yield similar, if poorly determined, values for the equilibrium RFIM exponents. The values for ν, γ and $\bar{\gamma}$ are consistent within the combined experimental and theoretical errors with most current theoretical predictions for the respective critical exponents of the 3D RFIM [35, 36]. Interestingly, the values for ν and γ agree within the errors with those of a pure Ising model in ~ 1.6 dimensions [37], consistent with the dimensional reduction argument of Villain [33] and Fisher [34].

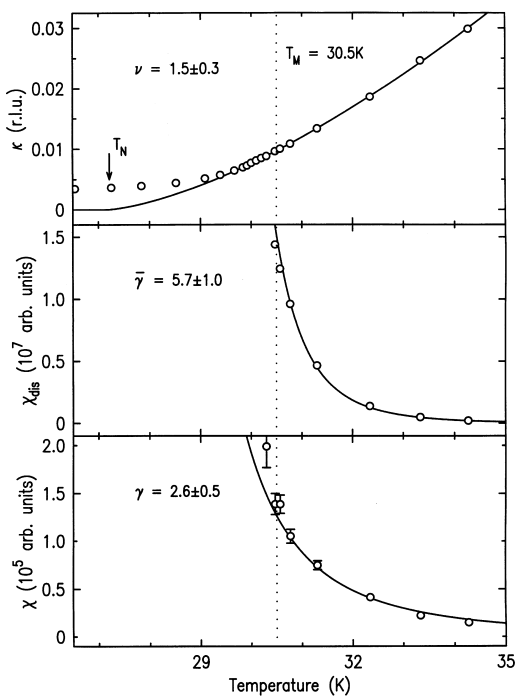

Fig. 13. Inverse correlation length κ, disconnected susceptibility χ_{dis}, and connected susceptibility χ as measured by neutron scattering for $Fe_{0.5}Zn_{0.5}F_2$ at 5 T. The dotted line shows the metastability temperature. T_N is the temperature at which the solid-line fit for κ reaches zero. The estimated critical exponents are given [14].

7. Conclusions

We now have a fairly complete empirical description of the equilibrium and nonequilibrium properties of several model RFIM systems. There appear to be no major contradictions between different classes of measurements on these materials. The application of synchrotron magnetic X-ray scattering techniques to this problem has clarified the behavior at large length scales and has provided the first reliable measurements of the order parameter, especially in the transition region. We also now have well-developed heuristic ideas which seem to describe successfully the overall dynamic behavior. However, a detailed quantitative theory for the equilibrium and nonequilibrium properties of the RFIM as well as the transition between these two behaviors is lacking. Clearly this represents an important challenge to all physicists interested in the behavior of systems with quenched disorder. Further experiments, especially on the equilibrium critical behavior, are also required.

These experiments illustrate clearly the role of model magnetic systems in condensed matter and statistical physics. As we noted in the Introduction to this paper, random-field effects are ubiquitous in condensed-matter materials. However, typically these systems are quite complicated and it is difficult to isolate those effects which arise purely from the random fields. Further, most often the random fields arise from quenched impurities so that one cannot easily vary the strength of the field in a given sample in order to deduce the quantitative dependence of the effects on the strength of the random field. By contrast, following the suggestion of Fishman and Aharony [5], it has been possible to explore thoroughly the physics of random fields using as 'laboratories' simple diluted or otherwise random two-sublattice Ising antiferromagnets. We anticipate that the field of Magnetism and such model magnetic systems will continue to play a central role in condensed-matter physics overall for the indefinite future.

First of all, we would like to thank the International Union of Pure and Applied Physics for honoring us with the IUPAP Magnetism Award 1997. This award, of course, honors not just ourselves but all of our collaborators. In addition, it recognizes our basic approach of using simple magnetic materials to elucidate the fundamental behavior of complex many-body systems. We would like to thank our collaborators in this RFIM work including A. Aharony, R.A. Cowley, Q. Feng, Q.J. Harris, J.P. Hill, A. Ito, A.P. Ramirez, G. Shirane, T.R. Thurston and H. Yoshizawa. We would also like to thank J. Als-Nielsen, Y. Endoh, M. Greven, H.J. Guggenheim, M.T. Hutchings, M.A. Kastner, K. Yamada and many others for their outstanding contributions overall to our studies of model magnetic systems. The research at MIT

was supported by the NSF under Grant No. DMR97-04532 and by the MRSEC Program of the National Science Foundation under Award No. DMR94-00334. Work at Brookhaven National Laboratory was carried out under Contract No. DE-AC276CH00016, Division of Material Science, US Department of Energy.

References

[1] A.I. Larkin, Sov. Phys. JETP 31 (1970) 784.
[2] Y. Imry, S.K. Ma, Phys. Rev. Lett. 35 (1975) 1399.
[3] J.Z. Imbrie, Phys. Rev. Lett. 53 (1984) 1747.
[4] J.Z. Imbrie, Commun. Math. Phys. 98 (1985) 145.
[5] S. Fishman, A. Aharony, J. Phys. C 12 (1979) L729.
[6] R.A. Cowley, H. Yoshizawa, G. Shirane, R.J. Birgeneau, Phys. Rev. B 30 (1984) 6650.
[7] R.J. Birgeneau, R.A. Cowley, G. Shirane, H. Yoshizawa, Phys. Rev. Lett. 54 (1985) 2147.
[8] R.A. Cowley, G. Shirane, H. Yoshizawa, Y.J. Uemura, R.J. Birgeneau, Z. Phys. B 75 (1989) 303.
[9] J.P. Hill, Q. Feng, R.J. Birgeneau, T.R. Thurston, Phys. Rev. Lett. 70 (1993) 3655.
[10] J.P. Hill, Q. Feng, R.J. Birgeneau, T.R. Thurston, Z. Phys. B 92 (1993) 285.
[11] R.J. Birgeneau, Q. Feng, Q.J. Harris, J.P. Hill, A.P. Ramirez, T.R. Thurston, Phys. Rev. Lett. 75 (1995) 1198.
[12] J.P. Hill, Q. Feng, Q.J. Harris, R.J. Birgeneau, A.P. Ramirez, A. Cassanho, Phys. Rev. B 55 (1997) 356.
[13] Q. Feng, R.J. Birgeneau, J.P. Hill, Phys. Rev. B 51 (1995) 15188.
[14] Q. Feng, Q.J. Harris, R.J. Birgeneau, J.P. Hill, Phys. Rev. B 55 (1997) 370.
[15] Q. Feng, A.P. Ramirez, Phys. Rev. B, in press.
[16] Q.J. Harris, Q. Feng, Y.S. Lee, R.J. Birgeneau, A. Ito, Phys. Rev. Lett. 78 (1997) 346.
[17] Q.J. Harris, Q. Feng, Y.S. Lee, Y.-J. Kim, R.J. Birgeneau, A. Ito, Z. Phys. B 102 (1997) 163.
[18] H. Yoshizawa, R.A. Cowley, G. Shirane, R.J. Birgeneau, H.J. Guggenheim, H. Ikeda, Phys. Rev. Lett. 48 (1982) 438.
[19] M. Hagen, R.A. Cowley, S.K. Satija, H. Yoshizawa, G. Shirane, R.J. Birgeneau, H.J. Guggenheim, Phys. Rev. B 28 (1983) 2602.
[20] Y. Shapira, N.F. Oliveira Jr., Phys. Rev. B 27 (1983) 4336.
[21] Y. Shapira, N.F. Oliveira Jr., S. Foner, Phys. Rev. B 30 (1984) 6639.
[22] J. Villain, Phys. Rev. Lett. 52 (1984) 1543.
[23] G.S. Grest, C.M. Soukoulis, K. Levin, Phys. Rev. B 33 (1986) 7659.
[24] G. Grinstein, J.F. Fernandez, Phys. Rev. B 29 (1984) 6389.
[25] R.A. Cowley, H. Yoshizawa, G. Shirane, R.J. Birgeneau, Z. Phys. B 58 (1984) 15.
[26] T. Natterman, I. Vilfan, Phys. Rev. Lett. 61 (1988) 223.
[27] M. Lederman, J.V. Selinger, R. Bruinsa, R. Orbach, J. Hommann, Phys. Rev. B 48 (1993) 3810.
[28] D.P. Belanger, A.R. King, V. Jaccarino, J.L. Cardy, Phys. Rev. B 28 (1983) 2522.
[29] I.B. Ferreira, A.R. King, V. Jaccarino, Phys. Rev. B 43 (1991) 70 797.
[30] I.B. Ferreira, Ph.D. Thesis, UCSB, Santa Barbara, CA, USA, 1992.
[31] P.-Z. Wong, Phys. Rev. Lett. 77 (1996) 2338.
[32] J.P. Hill, Q. Feng, R.J. Birgeneau, Phys. Rev. Lett. 77 (1996) 2339.
[33] J. Villain, J. Phys. (Paris) 46 (1985) 1843.
[34] D.S. Fisher, Phys. Rev. Lett. 56 (1986) 416.
[35] H. Reiger, Phys. Rev. B 52 (1995) 6651.
[36] M. Gofman, J. Adler, A. Aharony, A.B. Harris, M. Schwartz, Phys. Rev. Lett. 71 (1993) 1569 and references therein.
[37] M. Novotny, Phys. Rev. B 46 (1992) 2939.